# Computational Description of Alkylated Iron-Sulfur Organometallic Clusters

Richard J. Jodts, Mittkop, Madeline B. Ho, Milliam E. Broderick, Joan B. Broderick, Brian M. Hoffman, Martín A. Mosquera Martín A. Mosquera

<sup>1</sup>Department of Chemistry, Northwestern University, Evanston, Illinois 60208 <sup>2</sup>Department of Chemistry and Biochemistry, Montana State University, Bozeman, Montana 59717

Email: <u>bmh@northwestern.edu</u>
Email: <u>martinmosquera@montana.edu</u>

**Abstract:** The radical SAM enzyme superfamily has widespread roles in hydrogen atom abstraction reactions of crucial biological importance. In these enzymes, reductive cleavage of S-adenosyl methionine (SAM) bound to a [4Fe-4S]<sup>1+</sup> cluster generates the 5′-deoxyadenosyl radical (5′-dAdo•) which ultimately abstracts an H-atom from substrate. However, overwhelming experimental evidence has surprisingly revealed an obligatory organometallic intermediate  $\Omega$  exhibiting an Fe-C5′-adenosyl bond, whose properties are the target of this theoretical investigation. We report a readily-applied, 2-configuration version of BS-DFT, denoted 2C-DFT, designed to allow the accurate description of the hyperfine coupling constants and g-tensors of an alkyl group bound to a multi-metallic iron-sulfur cluster. This approach has been validated by the excellent agreement of its results both with those of multi-configurational CASSCF computations for a series of model complexes, and with the results from ENDOR/EPR spectroscopic studies for the crystallographically-characterized complex, M-CH<sub>3</sub>, a [4Fe-4S] cluster with an Fe-CH<sub>3</sub> bond. The likewise excellent agreement between spectroscopic results and 2C-DFT computations for  $\Omega$  validate its identity as an organometallic complex with a bond between an Fe of the [4Fe-4S] cluster and C5' of the deoxyadenosyl moiety, as first proposed.

## Introduction

Radical *S*-adenosyl-L-methionine (SAM) enzymes are ubiquitous amongst life, comprising one of the largest enzyme superfamilies. <sup>1</sup> <sup>2</sup> <sup>3,4</sup>. These enzymes catalyze the reductive cleavage of SAM by electron transfer from a [4Fe-4S]<sup>1+</sup> cluster to the sulfonium group of the coordinated SAM to form the highly reactive 5′-deoxyadenosyl radical (5′-dAdo•), which then ultimately abstracts a hydrogen atom from substrates. <sup>5</sup> <sup>6</sup> <sup>7</sup> However, rapid freeze-quench electron paramagnetic (EPR) and electron nuclear double resonance (ENDOR) spectroscopies have shown that prior to H-abstraction from substrate, 5′-dAdo• forms an organometallic intermediate, denoted  $\Omega$ , that is characterized by a direct bond between the [4Fe-4S]<sup>3+</sup> cluster and the 5′C of 5′-dAdo (**Figure 1**, **left**). <sup>8,9</sup> Later, it was shown that photo-reductive cleavage of SAM in a broad subset of radical SAM (RS) enzymes releases either 5′-dAdo• or a methyl radical (CH<sub>3</sub>•); <sup>5,10,11</sup> upon annealing, the latter forms an alternative organometallic species, denoted  $\Omega_{\rm M}$ , which was shown by ENDOR to have a [4Fe-4S]<sup>3+</sup> cluster with an Fe-CH<sub>3</sub> bond (**Figure 1**, **middle**). <sup>11</sup> <sup>10,12</sup> <sup>13</sup> Inspired by these discoveries, the M-CH<sub>3</sub> analogue of  $\Omega_{\rm M}$  (**Figure 1**, **right**) was synthesized and extensively characterized by crystallography as well as with Mossbauer and ENDOR spectroscopic methods, <sup>14,15</sup> with additional alkylated iron-sulfur clusters being synthesized and characterized. <sup>16</sup> <sup>17</sup> <sup>18</sup>

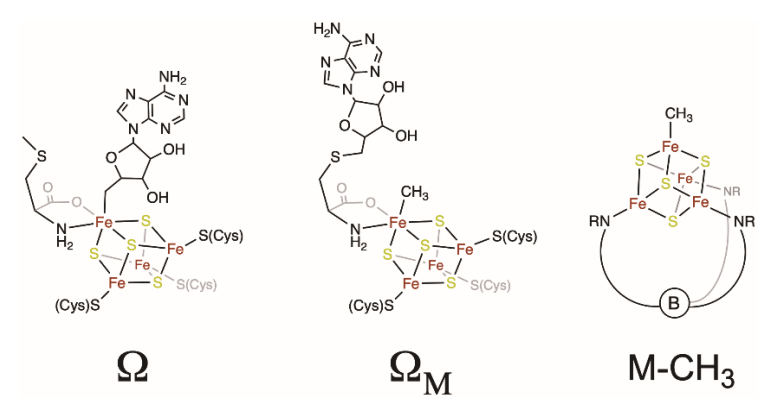


**Figure 1.** Representative structures of three [4Fe-4S] clusters with an alkylated unique iron. Here we show the proposed structure of the SAM intermediate  $\Omega$ , the proposed methyl bound analogue  $\Omega_{\rm M}$ , and the crystallographically determined synthetic M-CH<sub>3</sub>.

The discovery of these multi-metallic iron-sulfur organometallic complexes creates the necessity for accurate computation of their properties. The goal in this work is to devise a method to reliably describe a complex with an alkyl bound to a multi-metallic iron-sulfur cluster, to use this as a means of describing the properties of the crystallographically characterized M-CH<sub>3</sub>, and ultimately to probe the structures of the enzymatic intermediates  $\Omega$  and  $\Omega_M$ .

Multireference methods have become the cornerstone for capturing molecular properties, especially the complete active space self-consistent field (CASSCF) computational method, which has been shown to accurately replicate electronic structure and magnetic parameters derived from experiments. Multireference methods, unlike standard DFT, do not have issues with localization of metal electrons and incorporate electron-spin as a good quantum number, and thus are able to accurately replicate properties observed in experiment on metal complexes. However, currently it is impracticable to apply this approach to the [4Fe-4S] clusters, as their large number of localized electrons render them too computationally expensive.

The alternative approach, simple density functional theory (DFT) methods, is inadequate for the systems of interest, **Fig 1**, but the use of broken symmetry density functional theory (BS-DFT) has been shown to accurately capture the properties of [4Fe-4S] clusters as well as other iron-sulfur based clusters. <sup>19-22 23 24 25</sup> However, although 'simple' BS-DFT takes advantage of the ability of unrestricted standard DFT to render localized orbitals at each of the metal sites, it does not give wavefunctions of well-defined total spin, which is important in calculating the signature hyperfine coupling constant (HFCC) of nuclei of ligands bound to a multi-metallic iron-sulfur cluster

We here present a readily applied, 2-configuration version of BS-DFT, denoted 2-configuration DFT (2C-DFT), designed to allow the accurate description of an alkyl group bound to a multi-metallic iron-sulfur cluster, with a *focus* on computing the HFCCs for nuclei of the complex, which are commonly used in defining the molecular and electronic structure of an unknown system. This approach has been validated by the agreement of its results with those of high-level CASSCF computations for a series of model complexes, **Fig 2**, and with the spectroscopic results for the crystallographically-characterized complex, M-CH<sub>3</sub> (**Figs 1, 2**). 2C-DFT computations for  $\Omega$  are in excellent agreement with the spectroscopic properties of this intermediate, confirming its identity as an organometallic complex with a bond between an Fe of its [4Fe-4S] cluster and C5' of the deoxyadenosyl moiety, as first proposed.<sup>8</sup>

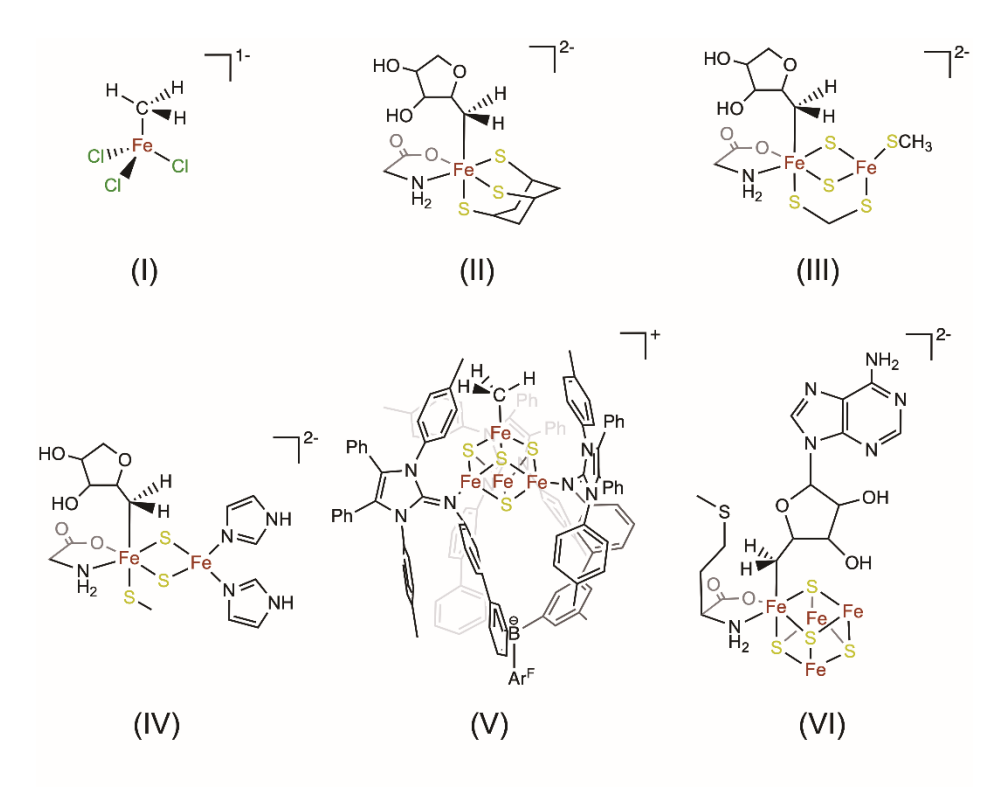


Figure 2 Structures considered in this work. I was previously studied by 3 Suess et al.  $^{14}$  II, III, and IV are systems that mimic the coordination of the unique iron, yet are not too complex for advanced methods. Structure V is a simplified illustration of the four-coordinate iron-methyl model synthesized and spectroscopically characterized previously (see SI for full model), and VI is the ENDOR derived/proposed Ω species structure, with cysteinyl ligands to the three cluster Fe truncated as CH<sub>3</sub>S-. (See SI for optimized coordinates of all model structures).  $^{14}$ 

#### **Computational Methods**

All computations were carried out in vacuo with the ORCA 4.2 program.<sup>26</sup> Geometry optimizations for all models described in Fig. 1 were performed using the BP86 exchange correlation functional and the relativistic zeroth order regular approximation (ZORA), where the atoms where assigned the ZORA-def2-TZVP basis set.<sup>27</sup> We also employ the D3 van der Waals correction, and the density fitting functionality SARC/J; samples of our input files can be found in the supporting information section. Employed also was the self-consistent field threshold "TightSCF" and optimization threshold "TightOpt". We use the regular convention of optimizing the molecular geometry with the iron clusters set in the high spin configuration, which offers a convenient balance of accuracy and computational speed. 28,29 With the optimized geometries obtained, we ran CASSCF and DFT calculations where the carbon ligated to the iron atom (denoted C<sub>1</sub> in the text and tables) and its <sup>1</sup>H atoms of interest are assigned the EPR-III basis set, otherwise other C and H atoms (including the following carbon bound to the C1 carbon, denoted C2) are described with the EPR-II basis set.<sup>30</sup> All Fe atoms are treated with the CP(PPP) set, and the S atoms have the def2-TZVP basis set applied to them.<sup>31</sup> The multireference CASSCF calculations were performed using a (7,6) active space [wherein for (n,m), n is the number of electrons and m the number of orbitals] for the monoiron models, and an active space of (13,11) for diiron systems. The DFT calculations performed for magnetic properties used the same basis set selection, in conjunction with the exchange coupling functionals BP86, or TPSSh.<sup>32</sup> <sup>33</sup> <sup>34</sup> <sup>35</sup> These two functionals are commonly employed for magnetic-property calculations.<sup>36</sup> Details of the standard treatments of the projection factors and isotropic hyperfine couplings are detailed in the text below and the SI.

## BS-DFT, Eigenstates of Total Spin, and calculation of HFCC for Fe-bound Alkyl complexes

In [4Fe-4S] clusters the spins localized on the metal ions are strongly coupled and a successful approach in describing this phenomenon is the Heisenberg-Dirac-van Vleck model (HDVV).<sup>20,21</sup> In the HDVV approach, a cluster is treated as a set of metallic spins with exchange couplings (and if necessary, double-exchange, and biquadratic couplings). As an example, the spin-Hamiltonian for a set of spins with J-coupling can be taken as:

$$H = \sum_{i>i} J_{ii} S_i S_i + \sum_i \mu_B B^T g_i S_i + \sum_{k,i} I_k^T A_{k,i} S_i,$$

$$\tag{1}$$

where the electron-spin sites within the molecule are labeled, i, j, and the nuclear spins, k. The gtensor of site i is given by the symbol  $g_i$ , whereas the hyperfine coupling tensor of electronic spin i to nucleus k is denoted as  $A_{k,i}$ . The hyperfine (k = i) tensor has isotropic and anisotropic components. The isotropic part is given by the well-known Fermi contact term. With careful coupling constant selection, this is a model that describes, in many cases very accurately, experimentally observable quantities associated with the cluster spin. Specifically, the HDVV theory is used to predict the spin configuration of a metallorganic cluster and the contribution of each spin site to the total spin of the system,  $^{20,21}$  which is key to understanding the HFCCs.

The BS-DFT wavefunction is a single multi-electron determinant that is not an eigenfunction of the total spin, and hence is not applicable for use in computing HFCCs. There are multiple ways to generate the eigenfunction of total spin from a BS-DFT wavefunction, which is required to achieve accurate HFCCs. An earlier approach for ligand site HFCCs, proposed by Noodleman et al., <sup>37</sup> <sup>38</sup> averages the product of the spin-coupling factors of the metallic sites, and uses the result to obtain HFCC to the ligand nuclei (absolute values). An alternative method suggested by Rapatskyi et al. <sup>39</sup> corresponds to simply summing over all products of spin-coupling factors (absolute value) to obtain the ligand HFCC. We propose an alternative theoretical approach in this work that leads to a simple, general prescription for treating the BS-DFT calculated hyperfine couplings of alkylated FeS clusters and show that it yields accurate ligand site hyperfine couplings by comparison to CASSCF computations on a suite of model complexes.

We define a 2-configuration DFT approach (2C-DFT) to achieving a wavefunction with total spin  $S_T = \frac{1}{2}$  as described visually in **Figure 3** and given by **eq 2**,

$$|\Psi\rangle = P_{\text{rad}}^{1/2} |\text{QS1}\rangle + P_{\text{cluster}}^{1/2} |\text{QS2}\rangle.$$
  $P_{\text{rad}} + P_{\text{cluster}} = 1;$   $P_{\text{rad}} << P_{\text{cluster}}$  (2)

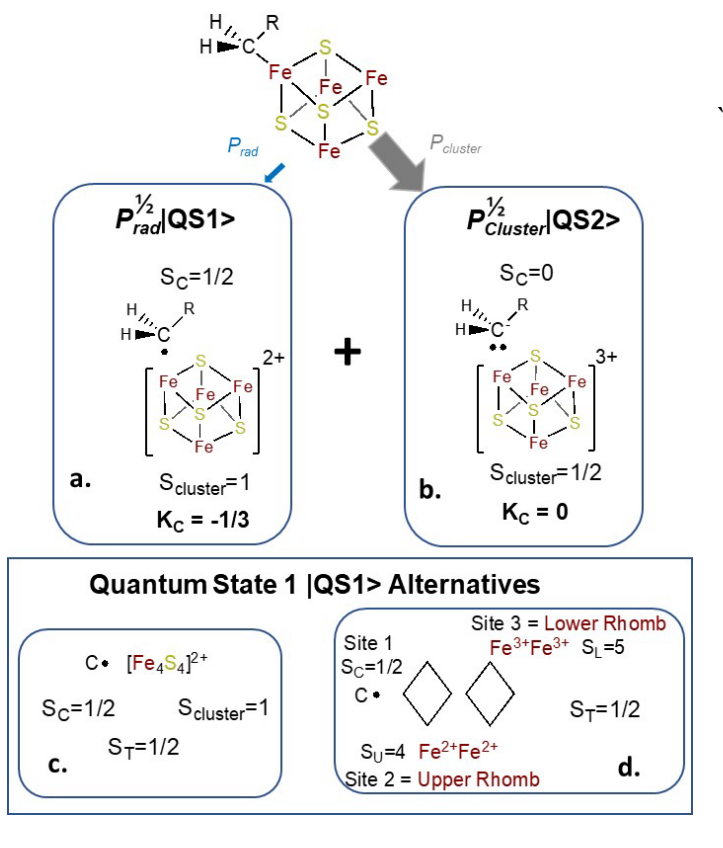


Figure 3. 2C-DFTmodel for the analysis of the HFCC of an alkyl bound to a [4Fe-4S] cluster. The wavefunction for the system is taken as a superposition of two states: a), quantum state 1, or QS1, with spin on the alkyl  $S_C = \frac{1}{2}$  and HFCC to the ligand nuclei, that is spin-coupled to a cluster with spin  $S_{\text{cluster}} = I$ , and **b**), quantum state 2, or QS2, where the alkyl group has  $S_C = 0$ , and does not exhibit ligand HFCC. c) shows a simple coupling scheme between alkyl with  $S_{\rm C}$ =  $\frac{1}{2}$  and 'monolithic' cluster with  $S_{\text{cluster}}$ = 1. d) defines a three-site model where the radical is coupled to a cluster comprised of two rhombs with total spins of, 4 and 5, respectively, spincouple to give  $S_{\text{cluster}} = I$ .

where  $P_{rad}$  and  $P_{cluster}$  are the probabilities of the QS1 and QS2 configurations, respectively. In the dominant configuration,  $|QS2\rangle$ , the cluster can be viewed as a  $[4Fe-4S]^{3+}$  cluster with  $S_{cluster} = \frac{1}{2}$ , while the C1 carbon of the organic moiety is anionic, closed-shell, and without spin. As a result, this configuration makes no contribution to the HF couplings to the alkyl spins, while the fact established below that  $P_{rad} << P_{cluster}$  allows us to compute  $^{57}Fe$  HFCCs by considering only the  $|QS2\rangle$   $[4Fe-4S]^{3+}$  cluster contribution .

Hyperfine couplings to the alkyl are introduced by the minority configuration,  $|QS1\rangle$ , which contains the  $[4Fe-4S]^{2+}$  cluster antiferromagnetically spin-coupled to the  $S_C = \frac{1}{2}$  neutral alkyl free-radical spin, which has hyperfine couplings to the alkyl nuclear spins. We formally assign the cluster in  $|QS1\rangle$  as being  $[4Fe-4S]^{2+}$ , with  $S_{cluster}=1$ . This excited-state contribution is induced by the interaction between the radical and the unique cluster Fe. It gives the best description of the BS-DFT results, as seen below when it is tested by comparison with CASSCF simulations and experiment.

Proceeding with  $|QS1\rangle$  thus described, in the simplest approach, it is straightforward to generate  $|QS1\rangle$  as an eigenfunction of total spin of the complex,  $S_T = \frac{1}{2}$  (wavefunctions,  $|QS1, S_T| = \frac{1}{2}$ ,  $m_T$ );  $m_T$  denoting the secondary spin quantum-number) through treatment of the complex as a two-spin entity, **Fig 3c**: a cluster with spin  $S_{\text{cluster}} = 1$  (wavefunctions  $|1, m_{\text{cl}}\rangle_{\text{cluster}}$ ,  $m_{\text{cl}}$  denoting the secondary spin quantum-number of the cluster) antiferromagnetically spin-coupled to the  $S_C = \frac{1}{2}$  radical (wavefunctions  $|\frac{1}{2}\rangle_{\text{cluster}}$ ,  $m_C\rangle_{\text{alkyl}}$ ,  $m_C$  denoting the secondary spin quantum-number of the radical). In this case the spin-coupled QS1 component of the 2C-DFT wavefunction is given by,

$$|QS1, \frac{1}{2}, +\frac{1}{2}\rangle = \sqrt{\frac{2}{3}} |1,1\rangle_{cluster} |\frac{1}{2}, -\frac{1}{2}\rangle_{alkyl} - \sqrt{\frac{1}{3}} |1,0\rangle_{cluster} |\frac{1}{2}, +\frac{1}{2}\rangle_{alkyl}$$
 (3)

with this component weighted in the 2C-DFT wavefunction (eq 2) by  $P_{\rm rad}^{1/2}$ .

As expressed in eq 1, we are interested in the full hyperfine coupling tensors, A, but we continue this analysis by focusing on the isotropic couplings as the clearest indication of bonding and the clearest metric to use in developing our new model for calculations; the same approach applies to the anisotropic HFCCs. The observed isotropic HFCC to nucleus  $I(a_i^{\text{obs}})$  of a complex with an alkyl moiety bonded to an Fe of a multi-metallic iron-sulfur cluster, total complex spin  $S_T$ , is incorporated in the hyperfine contribution to the complex's spin-Hamiltonian through a term involving the operators for the total complex spin ( $S_T$ ) and nuclear spin ( $I_i$ ),

$$H_i = a_i^{\text{obs}} S_{\text{T}} \bullet I_i \tag{4a}$$

whereas the intrinsic hyperfine coupling of the isolated (non-interacting) radical spin with the nucleus  $(a_i^{alk})$  is defined in terms of the operator for the local alkyl electron-spin  $(S^{alk})$ 

$$H_i^{\text{alk}} = a_i^{\text{alk}} \, \mathbf{S}^{\text{alk}} \, \bullet I_i \tag{4b}$$

The observed HF coupling parameter,  $a_i^{\text{obs}}$ , is determined in terms of the parameter for the isolated radical,  $a_i^{\text{alk}}$ , by the matrix element of the local alkyl electron-spin  $(S_z^{\text{alk}})$  with the spin-coupled QS1 wavefunction component (eq 3) as follows:

$$a_{i}^{\text{obs}} = P_{\text{rad}} \langle \text{QS1}, \frac{1}{2}, +\frac{1}{2} | 2a_{i}^{\text{alk}} S_{z}^{\text{alk}} | \text{QS1}, \frac{1}{2}, +\frac{1}{2} \rangle$$

$$= (-1/3) P_{\text{rad}} a_{i}^{\text{alk}}$$

$$\equiv K_{\text{C}} P_{\text{rad}} a_{i}^{\text{alk}}$$
(5)

Thus, use of the 2C-DFT wavefunction, eqs 2, 3, to compute  $a_i^{\text{obs}}$  gives a simple result, the product of three factors:  $K_C = -1/3$ , the coefficient that results from spin coupling within the exchange-coupled, QS1 configuration, and which weights the radical contribution to the total spin  $S_T = \frac{1}{2}$ ;  $P_{\text{rad}}$ , the contribution of the QS1 configuration to the total wavefunction; and  $a_i^{\text{alk}}$ , the hyperfine coupling to the nucleus of the isolated alkyl radical. However, the product of the latter two factors is accurately given by the straightforwardly computed BS-DFT coupling constant,  $a_i^{\text{BS}}$ , as the small net spin density on the bound alkyl site as determined by BS-DFT arises as the large local spin density of the pure radical multiplied by a small coefficient  $P_{\text{rad}}$ , This leads to the final prescription for use in comparing the 2C-DFT results for the alkyl-bound cluster to those from CASSCF and from experiment,

$$a_i^{\text{obs}} = K_{\text{C}} P_{\text{rad}} a_i^{\text{alk}}$$

$$\approx K_{\text{C}} a_i^{\text{BS}}$$
(6)

The excellent agreement of this equation with the results of CASSCF computations and with experiment, as shown below, confirms the inequality,  $P_{rad} << P_{cluster}$ , eq 2. as well as the final 2C-DFT prescription for comparing experiment and computation, Eq 6. In SI we present a more elegant, although perhaps less intuitively illuminating, derivation of eq 6.

Among several alternative views of spin-coupling in the cluster, we may follow Noodleman and Case<sup>19</sup> in treating the [4Fe-4S]<sup>2+</sup> cluster as two spin-coupled rhombs containing two Fe each, denoted upper (with the Fe-C bond) and lower, **Fig 3d**, where the rhombs are of intermediate spins, 4 and 5, and spin-coupled to give an overall cluster spin,  $S_{\text{cluster}} = I$ ; this cluster spin is then coupled with  $S_C = \frac{1}{2}$  to achieve the total system spin of  $S_T = \frac{1}{2}$ , as in the simpler approach of **Fig 3c**. Using the 2-rhomb approach, if we define the configurational quantum states as  $|S_C, S_U, S_{\text{cluster}}; S_T\rangle$ , then the two-configuration 2C-DFT wavefunction for the organometallic cluster becomes the eigenfunction of total spin  $S_T = \frac{1}{2}$ , eq 3

$$\left|\Psi, \frac{1}{2}\right\rangle = P_{\text{rad}}^{\frac{1}{2}} \left|\frac{1}{2}, 4, 1; \frac{1}{2}\right\rangle + P_{\text{cluster}}^{\frac{1}{2}} \left|0, \frac{9}{2}, \frac{1}{2}; \frac{1}{2}\right\rangle$$
 (7)

Although the spin coupling within this three-spin  $|QS1\rangle$  configuration with total spin  $S_T = \frac{1}{2}$  is more complex than the 2-spin case detailed above, as the spin-coupling between the cluster and radical is nonetheless the same, the resulting hyperfine coupling calculated for an alkyl nucleus is identical to that given by eq 6.

Of key importance, for multi-Fe systems the spin-coupling factor in **eqs 5** and **6** for the hyperfine coupling to an alkyl-spin is  $K_C = -1/3$ , and for the systems with a [4Fe-4S] cluster this is true regardless of whether the complex is taken as the two-spin system of **Fig 3c** or the three-spin system of **Fig 3d**. In short, the final 2C-DFT formula for the ligand site bound to a multi-Fe cluster, **eq 6**, is merely the product of the BS-DFT computed HFCC of the alkyl site  $(a_i^{BS})$ , and the factor  $K_C = -1/3$ , regardless of the description of the  $S_{cluster} = 1$  cluster. Thus, the 2C-DFT approach straightforwardly and universally introduces two extraordinarily significant corrections to the 'raw', single-determinantal, BS-DFT value for a ligand HFCC,  $a_i^{BS}$ : (i) the magnitude of the 2C-DFT HFCC is 1/3 that computed by BS-DFT; (ii) the sign of the HFCC in 2C-DFT is inverted from that given by BS-DFT. We validate the 2C-DFT approach through extensive comparisons to the results of high-level, multiconfigurational CASSCF computations on the model complexes of **Figure 2**, and then apply the method to the experimentally characterized complexes.

For completeness, it is important to further recognize that one can simply obtain the <sup>57</sup>Fe HFCC for the multi-iron systems (**Figure 2**) through the approach outlined for [4Fe-4S]<sup>3+</sup> clusters by Noodleman, which involves multiplication of the BS-DFT-computed  $a_{Fe}^{BS}$  by the vector-coupling coefficient, K, for Fe site i within the  $S_C = \frac{1}{2}$  total-spin cluster state, and the ratio,  $Ms_{total}/Ms_{site}$ , **eq 7**. For the diiron complexes in this study,  $K = +\frac{7}{3}$  for the <sup>57</sup>Fe(III) center. For the 4-iron systems we used  $K = +\frac{55}{27}$ , as derived by Noodleman, <sup>40</sup>

$$a_{\rm Fe}^{\rm obs} = K \frac{Ms_{\rm total}}{Ms_{\rm site}} a_{\rm Fe}^{\rm BS}$$
 (8)

Parenthetically, the result for the alkyl ligand to a monoiron complex is even simpler than eq 6. For the  $S_T = 5/2$  monoiron models, the 2C-DFT approach for the observed HFCC of the alkyl site simply 'collapses' to the raw DFT value ( $a_i^{\text{obs}} = a_i^{\text{DFT}}$ ). This is explained as follows: In the QS1 of the single iron systems  $S_C = 1/2$  and  $S_{\text{Fe}} = 2$ , then  $K_C = 1/5$ , but this factor is cancelled by the ratio of the total spin and alkyl site spin ( $Ms_{\text{total}}/Ms_{\text{site}} = 5$ ), so the raw BS-DFT HFCC of the alkyl site does not require a correction in these cases.

As a last remark about the 2C-DFT method, in principle, an S=1/2 alkylated cluster smoothly 'dissociates' the 'free' S=1/2 radical as the Fe-C distance is increased. In such dissociation, the "quantum state 1" picture becomes increasingly more dominant, and ultimately QS2 can be neglected. As required, the coupling of the radical to the cluster becomes weak at relatively long distances, and the contribution of the  $S_{\rm cluster}=1$  configuration, which would yield measurable <sup>57</sup>Fe HFCC, can be taken into account straightforwardly through quantum perturbation theory and 2C-DFT (with proper exchange-correlation functional selection), and the same for the HFCC couplings of the alkyl. At quite long distances, the radical and the cluster eventually decouple and the configuration with  $S_{\rm cluster}=0$  cluster and S=1/2 radical would completely describe the entire system.

# Validation of 2C-DFT through comparison to CASSCF computations on the models and to experiment

We have carried out both CASSCF and 2C-DFT computations for the model species I - IV depicted in Figure 1. We here compare the HFCCs computed by these two methods, and further compare them to those from raw BS-DFT and to the observed experimental HFFCs reported for  $\Omega$ , M-CH<sub>3</sub>, and  $\Omega$ <sub>M</sub> (**Table 1**; See SI for model coordinates).

Table 1: Isotropic HFCC for Observed Complexes								
(MHz)								
Molecule/site	$^{13}C_{1}$	<sup>57</sup> Fe	<sup>1</sup> H					
$\Omega^{8\;9}$	9	-34	8					
$M-CH_3^{14,15}$	+5.5		-8.5					
$\Omega_{ m M}^{11,13}$	+18							

Model I: To begin this computational study, we first examined an inorganic mono-iron model with a methyl group bound to an Fe(III), [FeCl<sub>3</sub>CH<sub>3</sub>]<sup>-1</sup> (I) (Fig. 2), the simplest model for the Fe-CH<sub>3</sub> bond of  $\Omega_{\rm M}$  and M-CH<sub>3</sub>. As mentioned above, the electronic structure of I was previously examined;14 here we extend the analysis methodologically to compute magnetic properties. For all the nuclei the differences between CASSCF and DFT couplings, which latter are merely equal to the raw DFT values as discussed subsequent to eq 8, are within the expected variation between methods, and are most likely due the inherent uncertainties of the common density functional approximations for metal systems. Using CASSCF (7,6) with the above described basis and functional, the calculated magnitudes of <sup>13</sup>C HFCC for the <sup>13</sup>C<sub>1</sub>, as well as the  $C_1$ - $^1$ H proton hyperfine coupling values in **I**, are in agreement with the  $^{13}$ C HFCC for  $\Omega_{\rm M}$  and the more extensive ENDOR data for the biomimetic organometallic complex M-CH<sub>3</sub> (Table 1); for I,  $a(^{13}C_1) \sim 17 \text{ MHz}$ ,  $a(^{1}H) = 11 \text{ MHz}$ , and  $a(^{57}Fe) = 4.7 \text{ MHz}$  is of expected magnitude (See Table 2). Use of either BP86 or TPSSh in calculating the BS-DFT coupling  $a_i^{BS}$ , yields  $a_i^{obs}$  for  $^{13}C_1$ and <sup>57</sup>Fe of I of comparable, if slightly higher, values than those given by the CASSCF method, and slightly lower values for the methyl proton HFCCs (Table 2). This agreement in the HFCCs for I calculated by both the CASSCF and BS-DFT methods validates the ability of DFT to describe

the Fe-alkyl bond, a foundational requirement for the 2C-DFT approach to alkyl complexes of multi-metallic iron-sulfur clusters, eq 6 and 8.

**Table 2.** Computed HFCCs (MHz) of the models described in **Figure 1**. CASSCF calculations with the active space (7,6) were carried out for **I** and **II**, whereas the active space (13,11) was used for **III** and **IV**, which involve two iron sites. The CASSCF calculations are run on the BP86-optimized molecular geometries. CASSCF is currently not applicable for V and VI. For all the models we report results from the BP86 DFT functional. Results from the TPSSh functional are shown in the **SI**. For easy interpretation we average the HFCCs of hydrogen sites. <sup>57</sup>Fe HFC listed in models III-VI refer to the alkyl-bound iron.

	CASSCF				2C-DFT (BP86)			
Molecule/site	$^{13}C_{1}$	$^{13}C_{2}$	<sup>57</sup> Fe	$^{1}\mathrm{H}_{\mathrm{avg}}$	$^{13}C_{1}$	$^{13}C_{2}$	<sup>57</sup> Fe	<sup>1</sup> H <sub>avg</sub>
I	17.0		4.7	11.0	14.4		8.1	4.3
II	10.3	1.4	18.4	12.5	15.7	2.5	10.5	0.6
III	2.9	1.0	20.5	5.1	10.9	0.2	19.2	2.7
IV	6.8	1.3	11.3	6.2	20.9	0.7	16.6	2.1
$\mathbf{V}$	Not	currently	applicable		+9.3		-10.1	-11.5
VI					+10.5	+0.1	-15.6	-1.3

Model II: Increasing the complexity of an monoiron-alkyl system, we examined a monoiron center II whose Fe exhibits the same direct coordination sphere as the alkylated Fe of  $\Omega$  and  $\Omega_M$ , particularly the direct C5′-Fe bond of  $\Omega$ . Again, CASSCF (7,6) computations (**Table 2**) for II yield both a  $^{13}$ C HFCC for the Fe-bound carbon and  $^{1}$ H HFCC for the C5′- $^{1}$ H protons, that are close to the experimental values found for the  $\Omega$  enzyme intermediates, and even roughly comparable to that measured for the structurally characterized M-CH<sub>3</sub> (**Table 1**). The BS-DFT calculations with the BP86 (**Table 2**) and TPSSh (**SI Table S1**) functionals give values for  $^{13}$ C<sub>1</sub>, in agreement with both CASSCF computations and experimental measurements on  $\Omega$ , and M-CH<sub>3</sub>, again validating the ability of BS-DFT to describe the Fe-alkyl bond.

The BS-DFT computed C5′-<sup>1</sup>H proton HFCC is slightly underestimated compared to the nonetheless small values observed for M-CH<sub>3</sub> and  $\Omega$  ( $a_{iso} = \sim 1$  MHz vs  $\sim 8$  MHz).<sup>15</sup> We attribute this discrepancy in **II**, which **I** did not have, to an effect of the higher coordination<sup>41</sup> of the unique iron of **II** reducing the delocalization of spin amongst the coordinated ligands, and thus decreasing the  $a_{i,site}$  factor of **eq 8**.

**Model III**: This is a Rieske-*inspired* diiron cluster model whose dominant configuration  $|QS2\rangle$  features an  $\Omega$ -like-coordinated Fe(III) antiferromagnetically coupled with a Fe(IV) partner site, a non-physical oxidation state that is adopted so that 5′-C is bonded to Fe(III); if the III/II valence is adopted, then the 5′-C becomes bonded to the Fe(II). Nonetheless, for this model both CASSCF and the 2C-DFT computation according to **eq 6** yield identical <sup>57</sup>Fe HFCCs for the alkyl-coordinated Fe. Overall, the 5′<sup>13</sup>C and 5′C-¹H HFCCs computed by the two methods essentially reproduce those observed experimentally in the structurally determined M-CH<sub>3</sub> complex (**IV**), and the 2C-DFT <sup>13</sup>C<sub>1</sub> HFCC exactly matches that of  $\Omega$ . In this case the ¹H couplings are equivalent for the two methods, while the <sup>13</sup>C couplings diverge somewhat (Table 2). Note, that if one simply applied the standard BS-DFT protocol for the HF coupling without incorporation of the factor,  $K_C$ 

= -1/3 (eq 6), the resultant coupling ( $a_{C1}^{BS}$  = 33 MHz) is far greater (4-fold!) than the value seen for omega.

Model IV: This is an  $\Omega$ -based Rieske system in which the dominant |QS2> configuration of the diiron center is the classical Fe(II)-Fe(III) spin-coupled pair, as is the case in biological diiron centers. This configuration is a simplified version of the [4Fe-4S] |QS2> spin-coupling configuration described in Fig 3d – with the upper rhomb represented by the spin-coupled Fe(II)/Fe(III) diiron pair and no lower rhomb. Both CASSCF and 2C-DFT computations resulted in a C<sub>1</sub>-Fe(III) bond as in the three experimentally studied organometallic complexes (Figure 1), and the magnitudes of all nuclear hyperfine couplings again are comparable for the two methods (Table 2). As with III, the CASSCF and 2C-DFT <sup>57</sup>Fe and <sup>1</sup>H HFCCs are in excellent agreement with the three experimentally explored [4Fe-4S] systems (Figure 1, Table 1 and 2), and likewise the 4′-<sup>13</sup>C (<sup>13</sup>C<sub>2</sub>) and beta-<sup>1</sup>H proton couplings, but with slight differences in <sup>13</sup>C<sub>1</sub> HFCCs. To perhaps belabor the point, once again the 'raw' BS-DFT produces values by themselves are too large for such a system: one cannot accurately capture the nature of a multi-iron system without incorporation of the factor,  $K_C$  (eq 6).

We conclude that the essential equivalence of the results of CASSCF and 2C-DFT computations, and the agreement with available experimental data from such systems, indeed validates the new, and readily implemented method for alkyl-bound multi-iron systems such as those of the biological intermediates. This contrasts with the failure of simple, uncorrected BS-DFT computations, whose magnitudes are three-fold greater because they lack the factor,  $K_C$  (eq 6). The benefit of 2C-DFT in calculating HFCC for the experimentally studied, alkylated 4Fe clusters of interest here, is that it provides a convenient and effective method for treating these clusters, which are beyond the current reach of CASSCF methods.

## 2C-DFT of experimentally observed alkylated-4Fe4S clusters.

We here apply the 2C-DFT method to the crystallographically characterized synthetic complex (M-CH<sub>3</sub>,  $\mathbf{V}$ ) and the key catalytic intermediate ( $\Omega$ ,  $\mathbf{VI}$ ), systems that are too complex for current application of the CASSCF multi-configuration calculations.

Complex V: Model V (Fig 2) is a model for the  $\Omega_{\rm M}$  enzymatic intermediate and a faithful representation of the synthetic, structurally characterized M-CH<sub>3</sub>, which furthermore has the most completely determined hyperfine couplings among the three current experimental systems (Fig 1).<sup>15</sup> To carry out two-rhomb computations for  $|{\rm QS1}\rangle$  (Fig 3d) one must first choose one of the other three Fe to partner with Fe1 as the upper rhomb when carrying out the 2C-DFT computation of V, which is equivalent to choosing which Fe spins are 'flipped' in constructing the BS-DFT wavefunction. However, it should not matter which of the other three is chosen because the three-fold symmetry around the four-coordinate unique Fe makes all three possible rhomb configurations essentially equivalent, and indeed, the three possible rhomb configurations do indeed produce essentially equivalent HFCC (Table S2).

As a foundational result, the 2C-DFT calculations of V, the [4Fe-4S]-CH<sub>3</sub> representation of M-CH<sub>3</sub> (**Fig 1**) gives  $g_{iso} > 2$  in agreement with experiment, an initial confirmation that this computational method accurately represents the observed electronic structure of M-CH<sub>3</sub>. The

magnitudes of the experimentally observed  $^{13}C_1$  and  $C_1$ - $^1H$  hyperfine coupling constants of M-CH<sub>3</sub> (**Table 1**) are well-reproduced by the calculated values (**Table 2**), even considering the slight overestimate of the  $^{13}C_1$  value. If one were instead to consider only a "pure" BS-DFT  $^{13}C_1$  HFCC results, omitting the required factor,  $K_C$  (eq 6), use of the optimal BP86 functional gives a coupling that is three-fold too large, and the discrepancy becomes even larger (five-fold) if one uses the suboptimal TPSSh functional (**SI Table S3**).

Of signal importance, the 2C-DFT  $^{13}$ C<sub>1</sub> HFCC has a positive sign, as experimentally determined for M-CH<sub>3</sub>, whereas pure BS-DFT HFCC yields a negative coupling, and as such qualitatively fails to reproduce experiment.  $^{57}$ Fe ENDOR was not collected on M-CH<sub>3</sub>, but the computed  $^{57}$ Fe HFCC for **V** are quite similar in magnitude to what was observed in the analogous  $\Omega$  experiments. These results demonstrate the ability of 2C-DFT to accurately describe the HFCC to the nuclei of an alkyl group bound to a crystallographically characterized [4Fe-4S] cluster, and the failure of simple BS-DFT to do so.

Complex VI: With a foundation of the computational validation of 2C-DFT and its success in describing the structurally characterized M-CH<sub>3</sub>, we now consider the representation of the catalytically central  $\Omega$  (VI) intermediate, with its six-coordinate, alkylated-iron site revealed through considerations of ENDOR-derived HFCCs. Unlike V, with three-fold symmetry at the Fe-CH<sub>3</sub>, for the six-coordinate unique iron of VI the three choices for upper rhomb within the cluster are no longer equivalent because the 3-fold symmetry has been lost. The best results (**Table** 1) are attained when treating the iron denoted as Fe2 as forming the upper rhomb (S=4) with Fe1 (see Figure S1 for iron labeling scheme and Table S2 for results of other rhomb configurations). Using this configuration of the [4Fe-4S] cluster and the BP86 functional, the resulting 2C-DFT calculation accurately reproduces the experimental g-tensor, with  $g_{iso} > 2$ , and  $g_{\parallel} > g_{\perp}$ , and reproduces with great accuracy the magnitude of the experimental <sup>13</sup>C<sub>1</sub> HFCC. Moreover, this methodology yields a positive <sup>13</sup>C<sub>1</sub> HFCC, which could not be measured but can be assumed based on the sign for the methyl-carbon coupling of M-CH<sub>3</sub>, as well as the sign obtained in  $\Omega_{\rm M}$ . It does equally well in reproducing the magnitude of the <sup>57</sup>Fe HFCC of the unique iron (again, the sign of the coupling presumed to be negative from  $\Omega_{\rm M}$  and M-CH<sub>3</sub>) (**Table 2**). Use of the TPPSh function not only yields magnitudes for the couplings that are somewhat too large for the <sup>13</sup>C<sub>1</sub>, but also gives the opposite sign compared to the BP86 (SI Table S3). Moreover, we note that the calculated C<sub>1</sub>-proton <sup>1</sup>H HFCC are themselves reasonably close to experiment in magnitude, although somewhat underestimated (~2 vs ~8 MHz, Table 1 and 2). The other possible rhomb configurations overestimate the magnitude of the <sup>13</sup>C<sub>1</sub> coupling, and therefore are eliminated as models to represent the actual Fe configurations of  $\Omega$  (Table S2).

Summary: The readily-applied 2C-DFT approach enables an accurate description of alkylbound multi-metallic iron-sulfur clusters, as validated by the excellent agreement of its results with those of the multi-reference CASSCF computations for the mono- and diiron models of **Fig 2**, and in particular by its strong agreement with the spectroscopic results for the crystallographically-characterized M-CH<sub>3</sub>, whose structure and Fe-CH<sub>3</sub> bond are well-modeled by  $\mathbf{V}$ , as well as its agreement with the results for  $\Omega$  itself. The success of the 2C-DFT approach reveals that the incorporation of a second determinantal configuration of the BS-DFT wavefunction (eq 2) provides a simple and accurate way to explicitly account for spin on the alkyl group, and thereby to attain accurate molecular properties, most notably the HFCCs (eqs 6, 8).

This report clearly shows it is inappropriate to use single-determinant BS-DFT approaches to investigate organometallic iron-sulfur clusters with an Fe-alkyl bond, such as presented recently in an errant attempt to treat  $\Omega$ . <sup>42</sup> Among the flaws in that report (which are discussed in detail in SI), it employed single-determinant BS-DFT computations that do not include the required projection factor,  $K_C = -I/3$ , which modifies the BS-DFT coupling in 2C-DFT, eq 6. As a result the reported HFCCs are *both* vastly overestimated *and* have the incorrect sign, which led to unfounded conclusions about the structure of  $\Omega$ .

Having confirmed that the 2C-DFT approach is able to reliably compute the hyperfine coupling constants for nuclei of an alkyl bound to a multi-metallic iron-sulfur cluster, the excellent agreement between spectroscopic results and the 2C-DFT computations for the  $\Omega$  model, VI, confirm that  $\Omega$  is indeed the organometallic complex visualized by VI and in Fig 1, with an Fe-C5'dAdo bond, as initially proposed<sup>2,8</sup> and as is increasingly accepted.<sup>43</sup>

**Acknowledgements:** We thank Dr. Hao Yang for discussions of his studies on  $\Omega_M$ , and Professor Daniel L. M. Suess for insightful comments on multi-Fe complexes such as M-CH<sub>3</sub>. M.A.M thanks MSU-Bozeman for startup support. M.W. acknowledges the support from the Out to Innovate 2021 Career Development Fellowship. M.A.M. and M.W. thank the Tempest High Performance Computing System, operated and supported by University Information Technology Research Cyberinfrastructure at Montana State University. R.J.J and M.B.H. were supported by the NIH (T32GM008382). B.M.H thanks the NIH (2 R01 GM111097) and NSF (MCB-1908587) for support. J.B.B. thanks the NIH (GM131889) for support. R.J.J. thanks Prof. George C. Schatz (Northwestern University) for use of his computational clusters, and R.J.J. and M.A.M. thank him for helpful discussion.

#### ASSOCIATED CONTENT

**Supporting Information**: The Supporting Information is available free of charge at <a href="https://pubs.acs.org">https://pubs.acs.org</a>

(Alkyl-Group couplings derived using the Wigner-Eckart theorem, TPSSh functional results, iron labeling scheme, all BS-DFT spin flips results, model coordinates used in calculations, and sample ORCA input scripts.)

#### AUTHOR INFORMATION

## **Corresponding Authors:**

Martin A. Mosquera - Department of Chemistry and Biochemistry, Montana State University, Bozeman, Montana 59717, United States; orcid.org/0000-0003-2170-5651 Email: martinmosquera@montana.edu

Brian M. Hoffman – Department of Chemistry, Northwestern University, Evanston, Illinois 60208, United States; orcid.org/0000-0002-3100-0746; Email: bmh@ northwestern.edu

#### **Authors:**

Richard J. Jodts – Department of Chemistry, Northwestern University, Evanston, Illinois 60208, United States; orcid.org/0000-0001-7467-492X

M Wittkop - Department of Chemistry and Biochemistry, Montana State University, Bozeman, Montana 59717, United States

Madeline B. Ho - Department of Chemistry, Northwestern University, Evanston, Illinois 60208, United States; <a href="https://orcid.org/0000-0001-6351-2132">https://orcid.org/0000-0001-6351-2132</a>

William E. Broderick: Department of Chemistry and Biochemistry, Montana State University, Bozeman, Montana 59717, United States; https://orcid.org/0000-0001-5782-7322

Joan B. Broderick: Department of Chemistry and Biochemistry, Montana State University, Bozeman, Montana 59717, United States; https://orcid.org/0000-0001-7057-9124

#### References

- (1) Broderick, J. B.; Duffus, B. R.; Duschene, K. S.; Shepard, E. M. Radical S-Adenosylmethionine Enzymes. *Chem Rev* **2014**, *114*, 4229-4317. DOI: 10.1021/cr4004709.
- (2) Broderick, J. B.; Broderick, W. E.; Hoffman, B. M. Radical Sam Enzymes: Nature's Choice for Radical Reactions. *FEBS Letters* **2023**, *597*, 92-101. DOI: https://doi.org/10.1002/1873-3468.14519.
- (3) Oberg, N.; Precord, T. W.; Mitchell, D. A.; Gerlt, J. A. Radicalsam.Org: A Resource to Interpret Sequence-Function Space and Discover New Radical Sam Enzyme Chemistry. *ACS Bio & Med Chem Au* **2022**, *2*, 22-35. DOI: 10.1021/acsbiomedchemau.1c00048.
- (4) Holliday, G. L.; Akiva, E.; Meng, E. C.; Brown, S. D.; Calhoun, S.; Pieper, U.; Sali, A.; Booker, S. J.; Babbitt, P. C.: Chapter One Atlas of the Radical Sam Superfamily: Divergent Evolution of Function Using a "Plug and Play" Domain. In *Methods Enzymol.*; Bandarian, V., Ed.; Academic Press, 2018; Vol. 606; pp 1-71.
- (5) Yang, H.; McDaniel, E. C.; Impano, S.; Byer, A. S.; Jodts, R. J.; Yokoyama, K.; Broderick, W. E.; Broderick, J. B.; Hoffman, B. M. The Elusive 5'-Deoxyadenosyl Radical: Captured and Characterized by Electron Paramagnetic Resonance and Electron Nuclear Double Resonance Spectroscopies. *J. Am. Chem. Soc.* **2019**, *141*, 12139-12146. DOI: 10.1021/jacs.9b05926.
- (6) Lundahl, M. N.; Sarksian, R.; Yang, H.; Jodts, R. J.; Pagnier, A.; Smith, D. F.; Mosquera, M. A.; van der Donk, W. A.; Hoffman, B. M.; Broderick, W. E.; Broderick, J. B. Mechanism of Radical S-Adenosyl-L-Methionine Adenosylation: Radical Intermediates and the Catalytic Competence of the 5'-Deoxyadenosyl Radical. *J. Am. Chem. Soc.* **2022**, *144*, 5087-5098. DOI: 10.1021/jacs.1c13706.
- (7) Sayler, R. I.; Stich, T. A.; Joshi, S.; Cooper, N.; Shaw, J. T.; Begley, T. P.; Tantillo, D. J.; Britt, R. D. Trapping and Electron Paramagnetic Resonance Characterization of the 5'dado• Radical in a Radical S-Adenosyl Methionine Enzyme Reaction with a Non-Native Substrate. *ACS Cent Sci* **2019**, *5*, 1777-1785. DOI: 10.1021/acscentsci.9b00706.
- (8) Horitani, M.; Shisler, K.; Broderick, W. E.; Hutcheson, R. U.; Duschene, K. S.; Marts, A. R.; Hoffman, B. M.; Broderick, J. B. Radical Sam Catalysis Via an Organometallic Intermediate with an Fe-[5'-C]-Deoxyadenosyl Bond. *Science* **2016**, *352*, 822-825. DOI: 10.1126/science.aaf5327.
- (9) Byer, A. S.; Yang, H.; McDaniel, E. C.; Kathiresan, V.; Impano, S.; Pagnier, A.; Watts, H.; Denler, C.; Vagstad, A. L.; Piel, J.; Duschene, K. S.; Shepard, E. M.; Shields, T. P.; Scott, L. G.; Lilla, E. A.; Yokoyama, K.; Broderick, W. E.; Hoffman, B. M.; Broderick, J. B. Paradigm Shift for Radical S-Adenosyl-L-Methionine Reactions: The Organometallic Intermediate Omega Is Central to Catalysis. *J. Am. Chem. Soc.* **2018**, *140*, 8634-8638. DOI: 10.1021/jacs.8b04061.
- (10) Impano, S.; Yang, H.; Jodts, R. J.; Pagnier, A.; Swimley, R.; McDaniel, E. C.; Shepard, E. M.; Broderick, W. E.; Broderick, J. B.; Hoffman, B. M. Active-Site Controlled, Jahn-Teller Enabled Regioselectivity in Reductive S-C Bond Cleavage of S-Adenosylmethionine in Radical Sam Enzymes. *J. Am. Chem. Soc.* **2021**, *143*, 335-348. DOI: 10.1021/jacs.0c10925.
- (11) Yang, H.; Impano, S.; Shepard, E. M.; James, C. D.; Broderick, W. E.; Broderick, J. B.; Hoffman, B. M. Photoinduced Electron Transfer in a Radical Sam Enzyme Generates an S-Adenosylmethionine Derived Methyl Radical. *J. Am. Chem. Soc.* **2019**, *141*, 16117-16124. DOI: 10.1021/jacs.9b08541.

- (12) Impano, S.; Yang, H.; Shepard, E. M.; Swimley, R.; Pagnier, A.; Broderick, W. E.; Hoffman, B. M.; Broderick, J. B. S-Adenosyl-L-Ethionine Is a Catalytically Competent Analog of S-Adenosyl-L-Methione (Sam) in the Radical Sam Enzyme Hydg. *Angew Chem Int Ed Engl* **2021**, *60*, 4666-4672. DOI: 10.1002/anie.202014337.
  - (13) Manuscript in preparation
- (14) McSkimming, A.; Sridharan, A.; Thompson, N. B.; Müller, P.; Suess, D. L. M. An [Fe<sub>4</sub>S<sub>4</sub>]<sup>3+</sup>–Alkyl Cluster Stabilized by an Expanded Scorpionate Ligand. *J. Am. Chem. Soc.* **2020**, *142*, 14314-14323. DOI: 10.1021/jacs.0c06334.
- (15) Ho, M. B.; Jodts, R. J.; Kim, Y.; McSkimming, A.; Suess, D. L. M.; Hoffman, B. M. Characterization by ENDOR Spectroscopy of the Iron–Alkyl Bond in a Synthetic Counterpart of Organometallic Intermediates in Radical Sam Enzymes. *J. Am. Chem. Soc.* **2022**, *144*, 17642-17650. DOI: 10.1021/jacs.2c07155.
- (16) Deng, L.; Holm, R. H. Stabilization of Fully Reduced Iron–Sulfur Clusters by Carbene Ligation: The  $[Fe_NS_N]^0$  Oxidation Levels (N = 4, 8). *J. Am. Chem. Soc.* **2008**, *130*, 9878-9886. DOI: 10.1021/ja802111w.
- (17) Ye, M.; Brown, A. C.; Suess, D. L. M. Reversible Alkyl-Group Migration between Iron and Sulfur in [Fe<sub>4</sub>S<sub>4</sub>] Clusters. *J. Am. Chem. Soc.* **2022**, *144*, 13184-13195. DOI: 10.1021/jacs.2c03195.
- (18) Brown, A. C.; Suess, D. L. M. Valence Localization in Alkyne and Alkene Adducts of Synthetic [Fe<sub>4</sub>S<sub>4</sub>]<sup>+</sup> Clusters. *Inorg. Chem.* **2022**. DOI: 10.1021/acs.inorgchem.2c01353.
- (19) Noodleman, L.; Case, D. A.: Local Density Functional Approaches to Spin Coupling in Transition Metal Clusters. In *Theory and Applications of Density Functional Approaches to Chemistry*; Labanowski, J. K., Andzelm, J. W., Eds.; Springer Verlag, 1991.
- (20) Noodleman, L.; Case, D. A.: Density-Functional Theory of Spin Polarization and Spin Coupling in Iron-Sulfur Clusters. In *Iron-Sulfur Proteins*; Cammack, R., Ed.; Advances in Inorganic Chemistry; Academic Press: San Diego, 1992; pp 423-470.
- (21) Noodleman, L.; Peng, C. Y.; Case, D. A.; Mouesca, J. M. Orbital Interactions, Electron Delocalization and Spin Coupling in Iron-Sulfur Clusters. *Coord. Chem. Rev.* **1995**, *144*, 199-244. DOI: 10.1016/0010-8545(95)07011-1.
- (22) Raugei, S.; Seefeldt, L. C.; Hoffman, B. M. Critical Computational Analysis Illuminates the Reductive-Elimination Mechanism That Activates Nitrogenase for N<sub>2</sub> Reduction. *PNAS* **2018**, *115*, E10521-E10530. DOI: 10.1073/pnas.1810211115.
- (23) Lovell, T.; Li, J.; Liu, T.; Case, D. A.; Noodleman, L. FeMo Cofactor of Nitrogenase: A Density Functional Study of States M<sup>n</sup>, M<sup>ox</sup>, M<sup>r</sup>, and M<sup>i</sup>. *J. Am. Chem. Soc.* **2001**, *123*, 12392-12410.
- (24) Mouesca, J. M.; Noodleman, L.; Case, D. A.; Lamotte, B. Spin-Densities and Spin Coupling in Iron-Sulfur Clusters a New Analysis of Hyperfine Coupling-Constants. *Inorg. Chem.* **1995**, *34*, 4347-4359. DOI: DOI 10.1021/ic00121a013.
- (25) Benediktsson, B.; Bjornsson, R. Quantum Mechanics/Molecular Mechanics Study of Resting-State Vanadium Nitrogenase: Molecular and Electronic Structure of the Iron–Vanadium Cofactor. *Inorg. Chem.* **2020**, *59*, 11514-11527. DOI: 10.1021/acs.inorgchem.0c01320.
- (26) Neese, F. The Orca Program System. *Wiley Interdisciplinary Reviews-Computational Molecular Science* **2012**, *2*, 73-78. DOI: Doi 10.1002/Wcms.81.
- (27) Lenthe, E. v.; Baerends, E. J.; Snijders, J. G. Relativistic Total Energy Using Regular Approximations. *J. Chem. Phys.* **1994**, *101*, 9783-9792. DOI: 10.1063/1.467943.

- (28) Terranova, U.; de Leeuw, N. H. Aqueous Fe<sub>2</sub>S2<sub>2</sub> Cluster: Structure, Magnetic Coupling, and Hydration Behaviour from Hubbard U Density Functional Theory. *Phys. Chem. Chem. Phys.* **2014**, *16*, 13426-13433. DOI: 10.1039/C4CP00984C.
- (29) Cox, N.; Ames, W.; Epel, B.; Kulik, L. V.; Rapatskiy, L.; Neese, F.; Messinger, J.; Wieghardt, K.; Lubitz, W. Electronic Structure of a Weakly Antiferromagnetically Coupled MnIIMnIIIModel Relevant to Manganese Proteins: A Combined Epr, <sup>55</sup>Mn-ENDOR, and DFT Study. *Inorg. Chem.* **2011**, *50*, 8238-8251. DOI: 10.1021/ic200767e.
- (30) Barone, V.; Bencini, A.; Ciofini, I.; Daul, C. A.; Totti, F. Density Functional Modeling of Couble Exchange Interactions in Transition Metal Complexes. Calculation of the Ground and Excited State Properties of [Fe<sub>2</sub>(OH)<sub>3</sub>(TmTacn)<sub>2</sub>]<sup>2+</sup>. *J. Am. Chem. Soc.* **1998**, *120*, 8357-8365.
- (31) Schafer, A.; Horn, H.; Ahlrichs, R. Fully Optimized Contracted Gaussian-Basis Sets for Atoms Li to Kr. *J. Chem. Phys.* **1992**, *97*, 2571-2577.
- (32) Becke, A. D. Density-Functional Exchange-Energy Approximation with Correct Asymptotic Behavior. *Physical Review A: Atomic, Molecular, and Optical Physics* **1988**, *38*, 3098-3100. DOI: 10.1103/PhysRevA.38.3098
- (33) Perdew, J. P. Density-Functional Approximation for the Correlation Energy of the Inhomogeneous Electron Gas. *Physical Review B* **1986**, *33*, 8822-8824. DOI: 10.1103/PhysRevB.33.8822.
- (34) Tao, J.; Perdew, J. P.; Staroverov, V. N.; Scuseria, G. E. Climbing the Density Functional Ladder: Nonempirical Meta--Generalized Gradient Approximation Designed for Molecules and Solids. *Phys. Rev. Lett.* **2003**, *91*, 146401. DOI: 10.1103/PhysRevLett.91.146401.
- (35) Neese, F. Prediction and Interpretation of the <sup>57</sup>Fe Isomer Shift in Mössbauer Spectra by Density Functional Theory. *Inorg. Chim. Acta* **2002**, *337*, 181-192. DOI: https://doi.org/10.1016/S0020-1693(02)01031-9.
- (36) Hedegård, E. D.; Kongsted, J.; Sauer, S. P. A. Improving the Calculation of Electron Paramagnetic Resonance Hyperfine Coupling Tensors for D-Block Metals. *Phys. Chem. Chem. Phys.* **2012**, *14*, 10669-10676. DOI: 10.1039/C2CP40969K.
- (37) Han, W.-G.; Liu, T.; Lovell, T.; Noodleman, L. Active Site Structure of Class I Ribonucleotide Reductase Intermediate X: A Density Functional Theory Analysis of Structure, Energetics, and Spectroscopy. *J. Am. Chem. Soc.* **2005**, *127*, 15778-15790.
- (38) Han, W. G.; Noodleman, L. Dft Calculations of Comparative Energetics and Endor/Mossbauer Properties for Two Protonation States of the Iron Dimer Cluster of Ribonucleotide Reductase Intermediate X. *Dalton Trans* **2009**, 6045-6057. DOI: 10.1039/b903847g.
- (39) Rapatskiy, L.; Ames, W. M.; Pérez-Navarro, M.; Savitsky, A.; Griese, J. J.; Weyhermüller, T.; Shafaat, H. S.; Högbom, M.; Neese, F.; Pantazis, D. A.; Cox, N. Characterization of Oxygen Bridged Manganese Model Complexes Using Multifrequency <sup>17</sup>O-Hyperfine EPR Spectroscopies and Density Functional Theory. *J. Phys. Chem. B* **2015**, *119*, 13904-13921. DOI: 10.1021/acs.jpcb.5b04614.
- (40) Noodleman, L. A Model for the Spin States of High-Potential Iron-Sulfur [Fe<sub>4</sub>S<sub>4</sub>]<sup>3+</sup> Proteins. *Inorg. Chem.* **1988**, *27*, 3677-3679. DOI: 10.1021/ic00293a051.
- (41) Johnson, E. R.; Otero-de-la-Roza, A.; Dale, S. G. Extreme Density-Driven Delocalization Error for a Model Solvated-Electron System. *J. Chem. Phys.* **2013**, *139*, 184116. DOI: 10.1063/1.4829642.

- (42) Donnan, P. H.; Mansoorabadi, S. O. Broken-Symmetry Density Functional Theory Analysis of the  $\Omega$  Intermediate in Radical S-Adenosyl-L-Methionine Enzymes: Evidence for a near-Attack Conformer over an Organometallic Species. *J. Am. Chem. Soc.* **2022**, *144*, 3381-3385. DOI: 10.1021/jacs.2c00678.
- (43) Balo, A. R.; Caruso, A.; Tao, L.; Tantillo, D. J.; Seyedsayamdost, M. R.; Britt, R. D. Trapping a Cross-Linked Lysine-Tryptophan Radical in the Catalytic Cycle of the Radical Sam Enzyme SuiB. *Proceedings of the National Academy of Sciences* **2021**, *118*, e2101571118. DOI: doi:10.1073/pnas.2101571118.

# TOC

